

# Analytical Approximate Solution for Double Ellipsoidal Heat Source in Finite Thick Plate

Analytical approximate solutions for double ellipsoidal heat sources in finite thick plate have been derived and calibrated with the experimental data

BY N. T. NGUYEN, Y.-W. MAI, S. SIMPSON, AND A. OHTA

## KEY WORDS

Double Ellipsoidal Heat Source  
 Single Ellipsoidal Heat Source  
 Gas Metal Arc Welding  
 Finite Body  
 Semi-Infinite Body  
 Analytical Approximate Solution

## Theoretical Analysis

### Temperature Field Solution Based on Green's Function for Instantaneous Point Source

Let us consider heat quantity  $\delta Q(x', y', z', t')$  acting instantaneously at time  $t'$  at point  $(x', y', z')$  in infinite body. The infinitesimal rise in temperature due to this point heat source  $dT(x, y, z, t')$  at point  $(x, y, z)$  and time  $t'$  in infinite body has been well established (Ref. 4) as

$$dT(x, y, z, t') = \frac{\delta Q(x', y', z', t') \cdot dt'}{\rho c [4\pi a(t-t')]^{3/2}} \cdot \exp\left[-\frac{(x-x')^2 + (y-y')^2 + (z-z')^2}{4a(t-t')}\right] \quad (1)$$

where  $dT(x, y, z, t')$  is an infinitesimal rise in temperature due to the point heat source  $\delta Q(x', y', z', t')$ ,  $\rho$  and  $c$  are mass density and specific heat,  $k$  is heat conduction coefficient, and  $a$  is thermal diffusivity ( $a = k/c\rho$ ).

Subsequently, the temperature field  $T(x, y, z, t)$  at time  $t$  for this point heat source  $\delta Q(x', y', z', t')$  can be obtained as

$$T(x, y, z, t) - T_o = \int_0^t \frac{\delta Q(x', y', z', t')}{\rho c} \cdot G_{inf}(x, y, z, t; x', y', z', t') dt' \quad (2)$$

where  $T_o$  is the initial temperature;  $G_{inf}(x, y, z, t; x', y', z', t')$  is the Green's function solution for the point source of unit magnitude in the infinite body, which is the temperature at point  $(x, y, z)$  and time  $t$  due to the instantaneous point source located at  $(x', y', z')$  at time  $t'$  and obtained as the solution to the heat conduction equation ( $\partial T/\partial t = a\nabla^2 T$ ) as

$$G_{inf}(x, y, z, t; x', y', z', t') dt' = \frac{1}{[4\pi a(t-t')]^{3/2}} \cdot \exp\left[-\frac{(x-x')^2 + (y-y')^2 + (z-z')^2}{4a(t-t')}\right] \quad (3)$$

Based on Equation 2, the temperature field for any kind of heat source [line heat source (1-D), surface heat source (2-D), or volume heat source (3-D)] in infinite body can be obtained by carry-

**ABSTRACT.** This work describes the detailed derivation of the analytical approximate solution for a double ellipsoidal density heat source in finite thick plate. This has shown that the solution of the heat source can be effectively used to predict the thermal history of the thick welded plate as well as weld pool shape geometry and various welding simulation purposes once the parameters of the heat source have been calibrated. This approximate solution can be directly used for welding simulation of finite thick plate without the need for implementing the mirror method as required in a semi-infinite body. Hence, it can be used as a potentially convenient tool for solving many problems in thermal stress analysis, residual stress analysis, and microstructure modeling of multipass welds, and others.

## Introduction

The temperature history of welded components has a significant influence on the residual stresses, distortion, and hence the fatigue behavior of welded structures. In order to obtain a good prediction for residual stress and distortion in welded joints and structures, an appropriate heat source is needed for that purpose.

Goldak et al. (Ref. 1) first introduced a three-dimensional (3-D) double ellipsoidal moving heat source and used finite element method (FEM) to calculate the temperature field of a bead on plate. He had shown that the 3-D heat source could overcome the shortcomings of the previous 2-D Gaussian model in order to predict the temperature of the welded joints with much deeper penetration. Nguyen et al. (Ref. 2) has recently developed a closed form analytical solution for this kind of 3-D heat source in a semi-infinite body and showed that this solution can be used for weld pool geometry prediction (Ref. 2) and for the calculation of residual stresses in a bead-on-plate weld (Ref. 3). However, the recent heat source solution is still limited to the semi-infinite body and one has to use the mirror image method when applying the solution for finite plates. This makes implementation of the solution a tedious task, especially for some complicated geometries.

In this paper, an analytical approximate solution for double ellipsoidal heat source in finite thick plate has been derived and calibrated with the experimental data.

N. T. NGUYEN is with ETRS Pty Ltd., Mulgrave, Australia. Y.-W. MAI is with Center for Advanced Materials & Technology (CAMT), School of Aerospace, Mechanical & Mechatronic Engineering, and S. SIMPSON is with School of Electrical and Information Engineering, The University of Sydney, Australia. A. OHTA is with Materials Strength and Life Evaluation Station, National Research Institute for Metals, Japan.

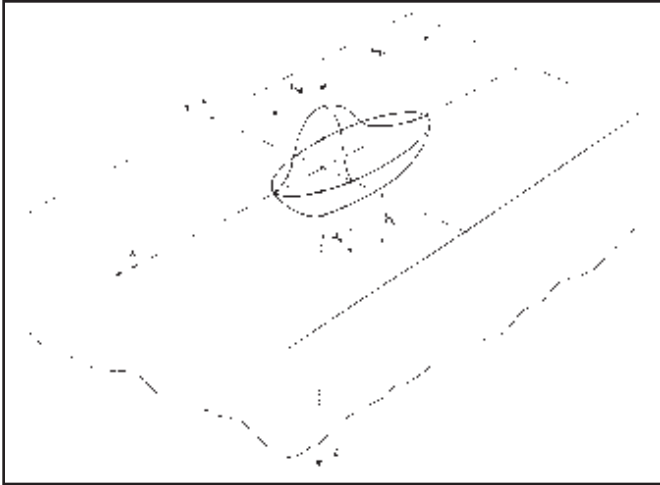


Fig. 1 — Double ellipsoidal power density distributed heat source.

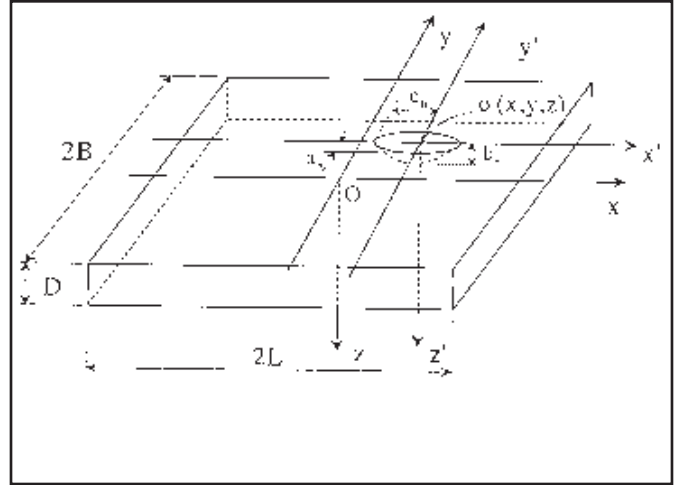


Fig. 2 — Single ellipsoidal heat source in a finite thick plate.

ing out the corresponding line, surface, or volume integration. For a volume distributed heat source with heat density  $Q(x',y',z',t')$  the temperature field in infinite body would be

$$T(x,y,z,t) - T_o = \iiint_V \int_0^t \frac{Q(x',y',z',t')}{\rho c} \bullet G_{inf}(x,y,z,t;x',y',z',t') dx' dy' dz' dt' \quad (4)$$

Note that this solution is based on Green's function for a point heat source in an infinite body. If a volume heat source in a finite body is considered, a new Green's function for a point heat source in the finite body that satisfies the Neumann boundary condition of zero heat density ( $\partial T/\partial n = 0$  where  $n$  is the normal direction) across its boundary surfaces should be adopted as

$$T(x,y,z,t) - T_o = \iiint_V \int_0^t \frac{Q(x',y',z',t')}{\rho c} \bullet G_{fin}(x,y,z,t;x',y',z',t') dx' dy' dz' dt' \quad (5)$$

where  $G_{fin}(x,y,z,t;x',y',z',t')$  is the Green's function for point heat source in finite body.

### Approximate Approach for Temperature Field Subjected to Volume Heat Source in Finite Body

It can be seen from Equation 5 that exact solutions for various kinds of heat sources in a finite body can be obtained if the Green's function for the point heat source in that particular body is known. However, the Green's function for the point heat source in a finite body would be expressed in a much more complicated form than that in an infinite body. Therefore, finding an analytical solution for Equation 5 would become an almost impossible task.

An alternative approximate approach to compensate for the Neumann boundary condition when dealing with a finite body is to keep using the same Green's function for the point source in an infinite body but replacing the heat source in an infinite body by the effective heat source  $Q_{eff}(x',y',z',t')$  in the finite body. The effective heat source should produce the same amount of heat input into the finite body as the original heat source would in an infinite body. This means that the amount of heat transferred in the whole infinite body now would rather be contained only in the finite

body. Subsequently, Equation 5 becomes

$$T(x,y,z,t) - T_o = \iiint_V \int_0^t \frac{Q_{eff}(x',y',z',t')}{\rho c} \bullet G_{inf}(x,y,z,t;x',y',z',t') dx' dy' dz' dt' \quad (6)$$

This approximate approach based on Equation 6 is reasonable as it is based on the two following assumptions:

- 1) The principle of conservation of energy for total heat input in infinite and finite bodies.
- 2) There is an insignificant effect of Green's functions for a point heat source in infinite and finite bodies on the shape of the distribution of the temperature field.

An example of deriving the exact conduction-only solution and approximate solution for the single ellipsoidal heat source in a semi-infinite body based on the above analysis is given in Appendix A. It has been shown that the Green's functions for point heat source in a semi-infinite body and a finite body do not change the shape of the temperature field, i.e., assumption 2 is correct in the case of a semi-infinite body.

Therefore, in this paper, this approximate approach has been implemented to obtain the analytical solution for a double ellipsoidal heat source in finite thick plate based on Equation 6.

## Ellipsoidal Heat Sources and Their Approximate Solution for Finite Plate

### Goldak's Ellipsoidal Heat Sources in Semi-Infinite Body

#### Single Ellipsoidal Heat Source

Goldak et. al. (Ref. 1) initially proposed a semi-ellipsoidal heat source in which heat density is distributed in a Gaussian manner throughout the heat source's volume. The heat density  $Q(x,y,z)$  at a point  $(x,y,z)$  within the semi-ellipsoid is given by the following equation:

$$Q(x,y,z) = \frac{6\sqrt{3\eta \bullet V \bullet I}}{a_h b_h c_h \pi \sqrt{\pi}} \exp\left(-\frac{3x^2}{c_h^2} - \frac{3y^2}{a_h^2} - \frac{3z^2}{b_h^2}\right) \quad (7)$$

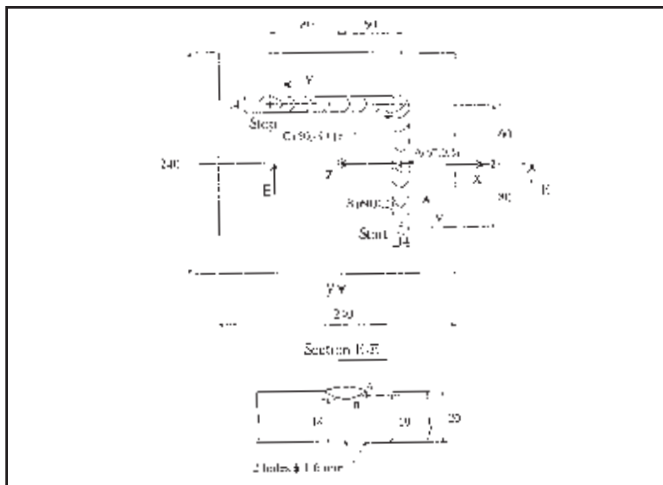


Fig. 3 — Specimen for transient temperature measurement.

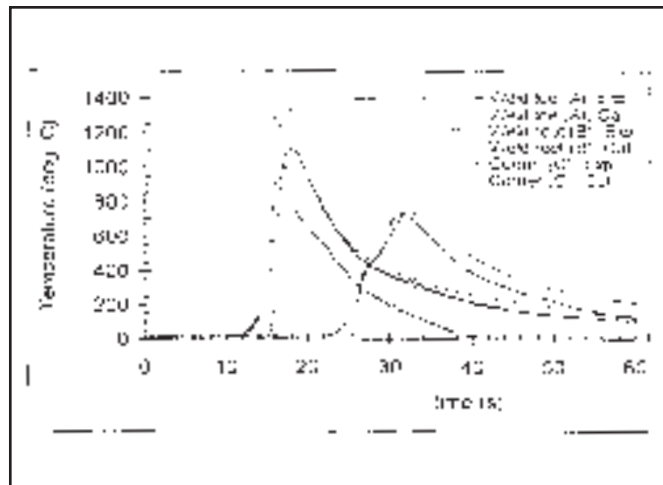


Fig. 4 — Calculated transient temperatures in comparison with the measured ones.

where  $a_h$ ,  $b_h$ , and  $c_h$  are ellipsoidal heat source parameters as described in Fig. 1 ( $c_{hf} = c_{hb} = c_h$ );  $x, y, z$  are moving coordinates of the heat source;  $Q(x, y, z)$  is heat density at a point  $(x, y, z)$ ;  $V$  and  $I$  are welding voltage and current, respectively, and  $\eta$  is arc efficiency.

### Goldak's Double Ellipsoidal Heat Source

Practical experience with the single heat source showed that the predicted temperature gradients in front of the arc were less steep than the experimentally observed ones, and gradients behind the arc were steeper than those measured. To overcome this, two ellipsoids were combined and proposed as a new heat source called "double ellipsoidal heat source" as shown in Fig. 1 (Ref. 1).

Since two different semi-ellipsoids are combined to give the new heat source, the heat density within each semi-ellipsoid are described by different equations. For a point  $(x, y, z)$  within the first semi-ellipsoid located in front of the welding arc, the heat density equation is described as

$$Q(x, y, z) = \frac{6\sqrt{3}r_f Q}{a_h b_h c_{hf} \pi \sqrt{\pi}} \exp\left(-\frac{3x^2}{c_{hf}^2} - \frac{3y^2}{a_h^2} - \frac{3z^2}{b_h^2}\right) \quad (8)$$

and for points  $(x, y, z)$  within the second semi-ellipsoid covering the rear section of the arc as

$$Q(x, y, z) = \frac{6\sqrt{3}r_b Q}{a_h b_h c_{hb} \pi \sqrt{\pi}} \exp\left(-\frac{3x^2}{c_{hb}^2} - \frac{3y^2}{a_h^2} - \frac{3z^2}{b_h^2}\right) \quad (9)$$

where  $a_h$ ,  $b_h$ ,  $c_{hf}$ , and  $c_{hb}$  are ellipsoidal heat source parameters as described in Fig. 1,  $Q$  is the heat input ( $Q = \eta IV$ ),  $r_f$  and  $r_b$  are proportion coefficients representing heat apportionment in front and back of the heat source, respectively ( $r_f + r_b = 2$ ).

It must be noted here that due to the continuity of the volumetric heat source, the values of  $Q(x, y, z)$  given by Equations 8 and 9 must be equal at the  $x = 0$  plane. From that condition, another constraint is obtained for  $r_f$  and  $r_b$  as  $r_f c_{hf} = r_b c_{hb}$ . Subsequently, the values for these two coefficients are determined as  $r_f = 2c_{hf}/(c_{hf} + c_{hb})$ ;  $r_b = 2c_{hb}/(c_{hf} + c_{hb})$ .

It is also worth noting here that this double ellipsoidal distrib-

ution heat source is described by five unknown parameters: the arc efficiency  $\eta$  and four ellipsoidal axes parameters,  $a_b$ ,  $b_b$ ,  $c_{hf}$ , and  $c_{hb}$ . Goldak et al. (Ref. 1) implied there is equivalence between the source dimensions and those of the weld pool and suggested that appropriate values for  $a_b$ ,  $b_b$ ,  $c_{hf}$ , and  $c_{hb}$  could be obtained by direct measurement of weld geometry.

### Effective Single Ellipsoidal Heat Sources in Finite Thick Plate

#### Single Ellipsoidal Heat Sources in Finite Thick Plate

Let us consider a single ellipsoidal heat source in a finite plate of width  $2B$ , length  $2L$ , and thickness  $D$ . The local coordinate of the heat source ( $O'x'y'z'$ ) is constructed so that its axes are parallel to the fixed coordinate of the finite plate ( $Oxyz$ ) as shown in Fig. 2 where origin  $O'$  is located at  $O'(x, y, z)$ .

Based on Goldak's heat source in a semi-infinite body, the single ellipsoidal heat source in finite plate is assumed to have the similar form but deferent maximum heat density magnitude as

$$Q_{eff}(x', y', z') = Q_{max} \exp\left(-\frac{3x'^2}{c_h^2} - \frac{3y'^2}{a_h^2} - \frac{3z'^2}{b_h^2}\right) \quad (10)$$

Furthermore, assuming that heat convection and radiation are ignorable due to the short time of welding in a quiet air environment, the conservation of energy in the finite plate requires that

$$2Q = 2Q_{max} \int_{-L-x}^{L-x} \int_{-B-y}^{B-y} \int_0^D \exp\left(-\frac{3x'^2}{c_h^2} - \frac{3y'^2}{a_h^2} - \frac{3z'^2}{b_h^2}\right) dx' dy' dz' \quad (11A)$$

or

$$Q = Q_{max} \int_{-L-x}^{L-x} \exp\left(-\frac{3x'^2}{c_h^2}\right) dx' \cdot \int_{-B-y}^{B-y} \exp\left(-\frac{3y'^2}{a_h^2}\right) dy' \int_0^D \exp\left(-\frac{3z'^2}{b_h^2}\right) dz' \quad (11B)$$

Equation 11B can be further simplified using the error function definition and rearranged for  $Q_{max}$  as

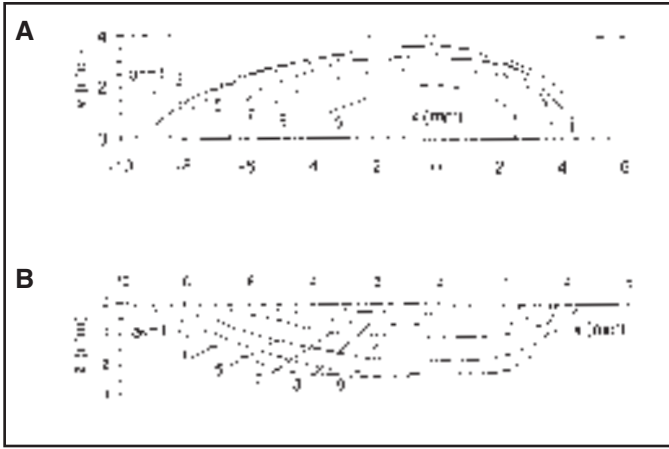


Fig. 5 — Effect of  $a_h$  on the weld pool geometry. A — Top view of the weld pool; B — longitudinal cross section of the weld pool.

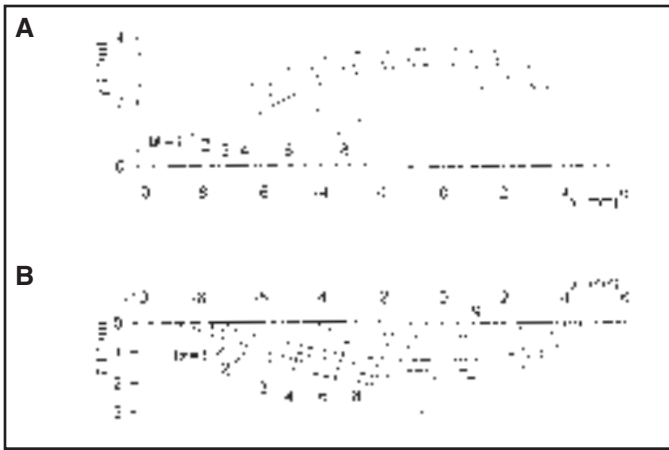


Fig. 6 — Effect of  $b_h$  on the weld pool geometry. A — Top view of the weld pool; B — longitudinal cross section of the weld pool.

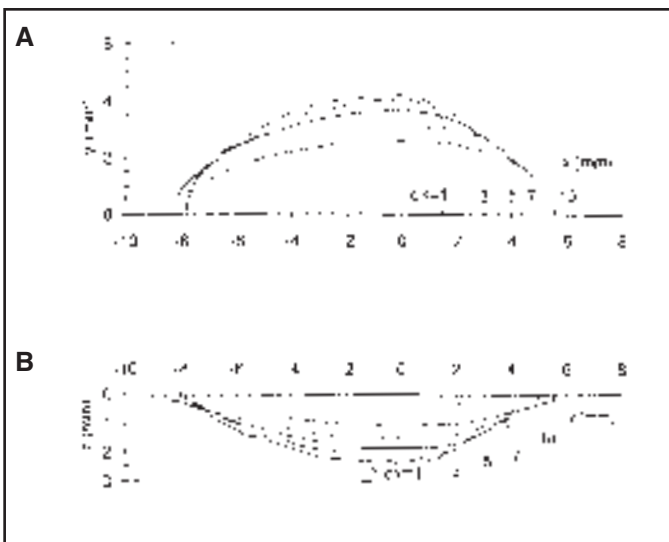


Fig. 7 — Effect of  $c_h$  on the weld pool geometry. A — Top view of the weld pool; B — longitudinal cross section of the weld pool.

$$Q_{max} = \frac{24Q\sqrt{3}}{\left[ \pi\sqrt{\pi a_h b_h c_h} \operatorname{erf}\left(\frac{D\sqrt{3}}{c_h}\right) \cdot \left( \operatorname{erf}\left(\frac{(L-x)\sqrt{3}}{c_h}\right) + \operatorname{erf}\left(\frac{(L+x)\sqrt{3}}{c_h}\right) \right) \cdot \left( \operatorname{erf}\left(\frac{(B-y)\sqrt{3}}{a_h}\right) + \operatorname{erf}\left(\frac{(B+y)\sqrt{3}}{a_h}\right) \right) \right]} \quad (12)$$

Substituting Equation 12 into Equation 10 gives the heat density equation for the proposed single ellipsoidal heat source in the finite plate as

$$Q_{eff}(x', y', z') = \frac{24Q\sqrt{3} \exp\left(-\frac{3x'^2}{c_h^2} - \frac{3y'^2}{a_h^2} - \frac{3z'^2}{b_h^2}\right)}{\left[ \pi\sqrt{\pi a_h b_h c_h} \operatorname{erf}\left(\frac{D\sqrt{3}}{c_h}\right) \cdot \left( \operatorname{erf}\left(\frac{(L-x)\sqrt{3}}{c_h}\right) + \operatorname{erf}\left(\frac{(L+x)\sqrt{3}}{c_h}\right) \right) \cdot \left( \operatorname{erf}\left(\frac{(B-y)\sqrt{3}}{a_h}\right) + \operatorname{erf}\left(\frac{(B+y)\sqrt{3}}{a_h}\right) \right) \right]} \quad (13)$$

### Analytical Approximate Solution for Single Ellipsoidal Heat Source in Finite Thick Plate

Let us consider a finite plate of width  $2B$ , length  $2L$ , and thickness  $D$  as in Fig. 2 again. The approximate solution for the single ellipsoidal heat source in this finite thick plate is based on the approach described in the section titled "Approximate Approach for Temperature Field Subjected to Volume Heat Source in Finite Body." Substituting Equations 3 and 10 into Equation 5 and rearranging the variables gives

$$T(x, y, z, t) - T_o = \int_0^t \frac{Q_{max} dt'}{\rho c [4\pi a(t-t')]^{3/2}} \int_{-L-x}^{L-x} \exp\left(-\frac{3x'^2}{c_h^2} - \frac{(x-x')^2}{4a(t-t')}\right) dx' \cdot \int_{-B-y}^{B-y} \exp\left(-\frac{3y'^2}{a_h^2} - \frac{(y-y')^2}{4a(t-t')}\right) dy' \cdot \int_0^D \exp\left(-\frac{3z'^2}{b_h^2} - \frac{(z-z')^2}{4a(t-t')}\right) dz' \quad (14A)$$

or

$$T(x, y, z, t) - T_o = \int_0^t \frac{Q_{max} dt'}{\rho c [4\pi a(t-t')]^{3/2}} I_L I_B I_D \quad (14B)$$

where

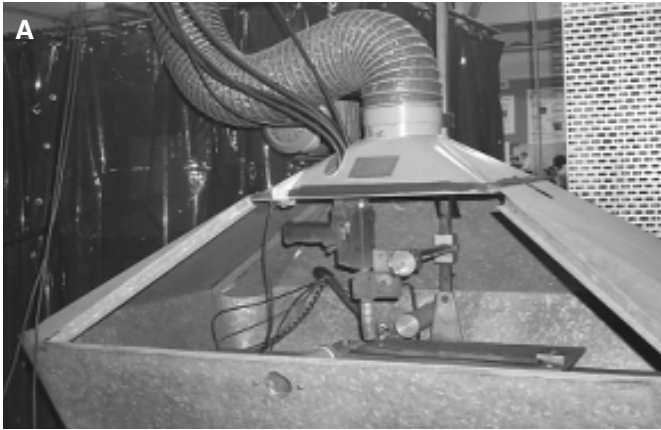


Fig. 8 — Experimental setup for specimen fabrication and data acquisition. A — Welding system for specimen fabrication; B — data logging system using WeldPrint software.

$$I_L = \int_{-L-x}^{L-x} \exp\left(-\frac{3x'^2}{c_h^2} - \frac{(x-x')^2}{4a(t-t')}\right) dx'$$

$$I_B = \int_{-B-y}^{B-y} \exp\left(-\frac{3y'^2}{a_h^2} - \frac{(y-y')^2}{4a(t-t')}\right) dy'$$

$$I_D = \int_0^D \exp\left(-\frac{3z'^2}{b_h^2} - \frac{(z-z')^2}{4a(t-t')}\right) dz'$$

$$I_D = \exp\left(-\frac{3z^2}{12a(t-t') + b_h^2}\right) \cdot \frac{b_h \sqrt{4a(t-t')}}{\sqrt{12a(t-t') + b_h^2}}$$

$$\cdot \frac{\sqrt{\pi}}{2} \left[ \operatorname{erf}\left(\frac{12a(t-t')D + b_h^2(D-z)}{b_h \sqrt{4a(t-t')} \sqrt{12a(t-t') + b_h^2}}\right) + \operatorname{erf}\left(\frac{b_h z}{\sqrt{4a(t-t')} \sqrt{12a(t-t') + b_h^2}}\right) \right] \quad (15C)$$

Integrals  $I_L$ ,  $I_B$ , and  $I_D$  can be solved using the error function notation as

$$I_L = \exp\left(-\frac{3x^2}{12a(t-t') + c_h^2}\right) \cdot \frac{c_h \sqrt{4a(t-t')}}{\sqrt{12a(t-t') + c_h^2}}$$

$$\cdot \frac{\sqrt{\pi}}{2} \left[ \operatorname{erf}\left(\frac{(12a(t-t') + c_h^2)(L-x) - c_h^2 x}{c_h \sqrt{4a(t-t')} \sqrt{12a(t-t') + c_h^2}}\right) + \operatorname{erf}\left(\frac{(12a(t-t') + c_h^2)(L+x) - c_h^2 x}{c_h \sqrt{4a(t-t')} \sqrt{12a(t-t') + c_h^2}}\right) \right] \quad (15A)$$

$$I_B = \exp\left(-\frac{3y^2}{12a(t-t') + a_h^2}\right) \cdot \frac{a_h \sqrt{4a(t-t')}}{\sqrt{12a(t-t') + a_h^2}}$$

$$\cdot \frac{\sqrt{\pi}}{2} \left[ \operatorname{erf}\left(\frac{(12a(t-t') + a_h^2)(B-y) - a_h^2 y}{a_h \sqrt{4a(t-t')} \sqrt{12a(t-t') + a_h^2}}\right) + \operatorname{erf}\left(\frac{(12a(t-t') + a_h^2)(B+y) - a_h^2 y}{a_h \sqrt{4a(t-t')} \sqrt{12a(t-t') + a_h^2}}\right) \right] \quad (15B)$$

Substituting Equations 12 and 15A–C into Equation 14B and subsequently simplifying gives

$$T(x, y, z, t) - T_o = \frac{3\sqrt{3}Q}{\rho c \pi \sqrt{\pi}}$$

$$\cdot \int_0^t \frac{E(L, x, c_h) \cdot E(B, y, a_h) \cdot E(D, z, b_h)}{\sqrt{12a(t-t') + a_h^2} \sqrt{12a(t-t') + b_h^2} \sqrt{12a(t-t') + c_h^2}}$$

$$\cdot \exp\left(-\frac{3x^2}{12a(t-t') + c_h^2} - \frac{3y^2}{12a(t-t') + a_h^2} - \frac{3z^2}{12a(t-t') + b_h^2}\right) dt' \quad (16A)$$

where

$$E(L, x, c_h) = \frac{\left[ \operatorname{erf}\left(\frac{(12a(t-t') + c_h^2)(L-x) - c_h^2 x}{c_h \sqrt{4a(t-t')} \sqrt{12a(t-t') + c_h^2}}\right) + \operatorname{erf}\left(\frac{(12a(t-t') + c_h^2)(L+x) - c_h^2 x}{c_h \sqrt{4a(t-t')} \sqrt{12a(t-t') + c_h^2}}\right) \right]}{\left[ \operatorname{erf}\left(\frac{(L-x)\sqrt{3}}{c_h}\right) + \operatorname{erf}\left(\frac{(L+x)\sqrt{3}}{c_h}\right) \right]} \quad (16B)$$

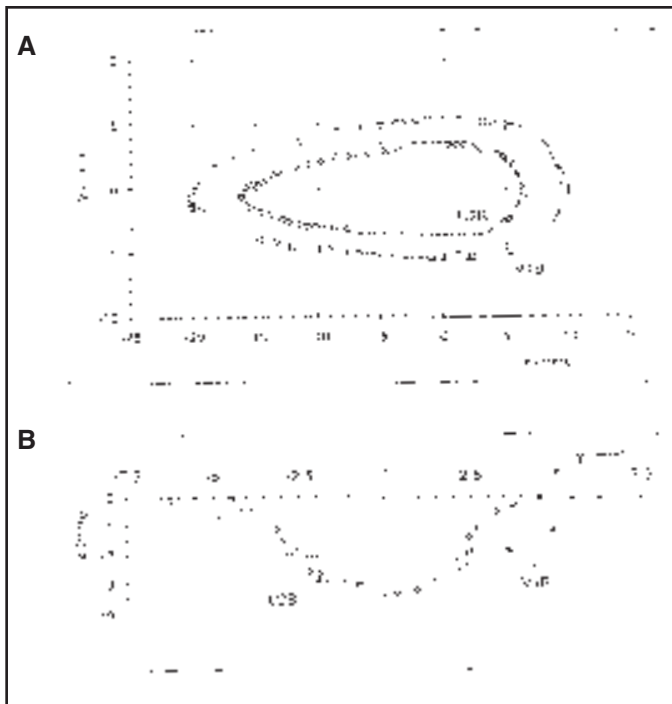


Fig. 9 — Comparisons between the measured and the predicted weld pool shape. A — Top view of the weld pool shape; B — transversal cross section of the weld pool.

$$E(B, y, a_h) = \frac{\left[ \begin{aligned} &\operatorname{erf} \left( \frac{(12a(t-t') + a_h^2)(B-y) - a_h^2 y}{a_h \sqrt{4a(t-t') \sqrt{12a(t-t') + a_h^2}}} \right) \\ &+ \operatorname{erf} \left( \frac{(12a(t-t') + a_h^2)(B+y) - a_h^2 y}{a_h \sqrt{4a(t-t') \sqrt{12a(t-t') + a_h^2}}} \right) \end{aligned} \right]}{\left[ \operatorname{erf} \left( \frac{(B-y)\sqrt{3}}{a_h} \right) + \operatorname{erf} \left( \frac{(B+y)\sqrt{3}}{a_h} \right) \right]} \quad (16C)$$

$$E(D, z, b_h) = \frac{\left[ \begin{aligned} &\operatorname{erf} \left( \frac{12a(t-t')D + b_h^2(D-z)}{b_h \sqrt{4a(t-t') \sqrt{12a(t-t') + b_h^2}}} \right) \\ &+ \operatorname{erf} \left( \frac{b_h z}{\sqrt{4a(t-t') \sqrt{12a(t-t') + b_h^2}}} \right) \end{aligned} \right]}{\bullet \operatorname{erf}^{-1} \left( \frac{D\sqrt{3}}{b_h} \right)} \quad (16D)$$

Finally, substituting  $x = x - vt'$  (for the moving heat source with constant speed  $v$  in  $x$ -direction) to Equations 16A and B gives the final approximate solution for the moving heat source in a finite thick plate as

$$T(x, y, z, t) - T_o = \frac{3\sqrt{3}Q}{\rho c \pi \sqrt{\pi}} \int_0^t \frac{E(L, x - vt', c_h) \bullet E(B, y, a_h) \bullet E(D, z, b_h)}{\sqrt{12a(t-t') + a_h^2} \sqrt{12(t-t') + b_h^2} \sqrt{12a(t-t') + c_h^2}} \bullet \exp \left( - \frac{3(x-vt')^2}{12a(t-t') + c_h^2} - \frac{3y^2}{12a(t-t') + a_h^2} - \frac{3z^2}{12a(t-t') + b_h^2} \right) dt' \quad (17)$$

It is worth noting here that the approximate solution obtained for the moving single ellipsoidal heat source in finite plate as given by Equation 17 is of the similar form as that obtained earlier by Nguyen et al. (Ref. 2) for the heat source in semi-infinite body, except for the error function correction terms  $[E(L, x-vt'), E(B, y), \text{ and } E(D, z)]$  due to plate length, width, and thickness, respectively.

### Effective Double Ellipsoidal Heat Sources in Finite Plate

#### Double Ellipsoidal Heat Sources in Finite Plate

Let us now consider that the heat source consists of two quarters of different ellipsoids as shown in Fig. 1. Following a similar procedure as described in the previous section for the single ellipsoidal heat source, density equations are obtained for the front and back half of the double ellipsoidal heat source, respectively as follows

$$Q_{f,eff}(x', y', z') = \frac{24Qr_f \sqrt{3} \exp \left( - \frac{3x'^2}{c_{hf}^2} - \frac{3y'^2}{a_h^2} - \frac{3z'^2}{b_h^2} \right)}{\left[ \begin{aligned} &\pi \sqrt{\pi} a_h b_h c_{hf} \operatorname{erf} \left( \frac{D\sqrt{3}}{b_h} \right) \\ &\bullet \left( \operatorname{erf} \left( \frac{(L-x)\sqrt{3}}{c_{hf}} \right) + \operatorname{erf} \left( \frac{(L+x)\sqrt{3}}{c_{hf}} \right) \right) \\ &\bullet \left( \operatorname{erf} \left( \frac{(B-y)\sqrt{3}}{a_h} \right) + \operatorname{erf} \left( \frac{(B+y)\sqrt{3}}{a_h} \right) \right) \end{aligned} \right]} \quad (18A)$$

$$Q_{b,eff}(x', y', z') = \frac{24Qr_b \sqrt{3} \exp \left( - \frac{3x'^2}{c_{hb}^2} - \frac{3y'^2}{a_h^2} - \frac{3z'^2}{b_h^2} \right)}{\left[ \begin{aligned} &\pi \sqrt{\pi} a_h b_h c_{hb} \operatorname{erf} \left( \frac{D\sqrt{3}}{b_h} \right) \\ &\bullet \left( \operatorname{erf} \left( \frac{(L-x)\sqrt{3}}{c_{hb}} \right) + \operatorname{erf} \left( \frac{(L+x)\sqrt{3}}{c_{hb}} \right) \right) \\ &\bullet \left( \operatorname{erf} \left( \frac{(B-y)\sqrt{3}}{a_h} \right) + \operatorname{erf} \left( \frac{(B+y)\sqrt{3}}{a_h} \right) \right) \end{aligned} \right]} \quad (18B)$$

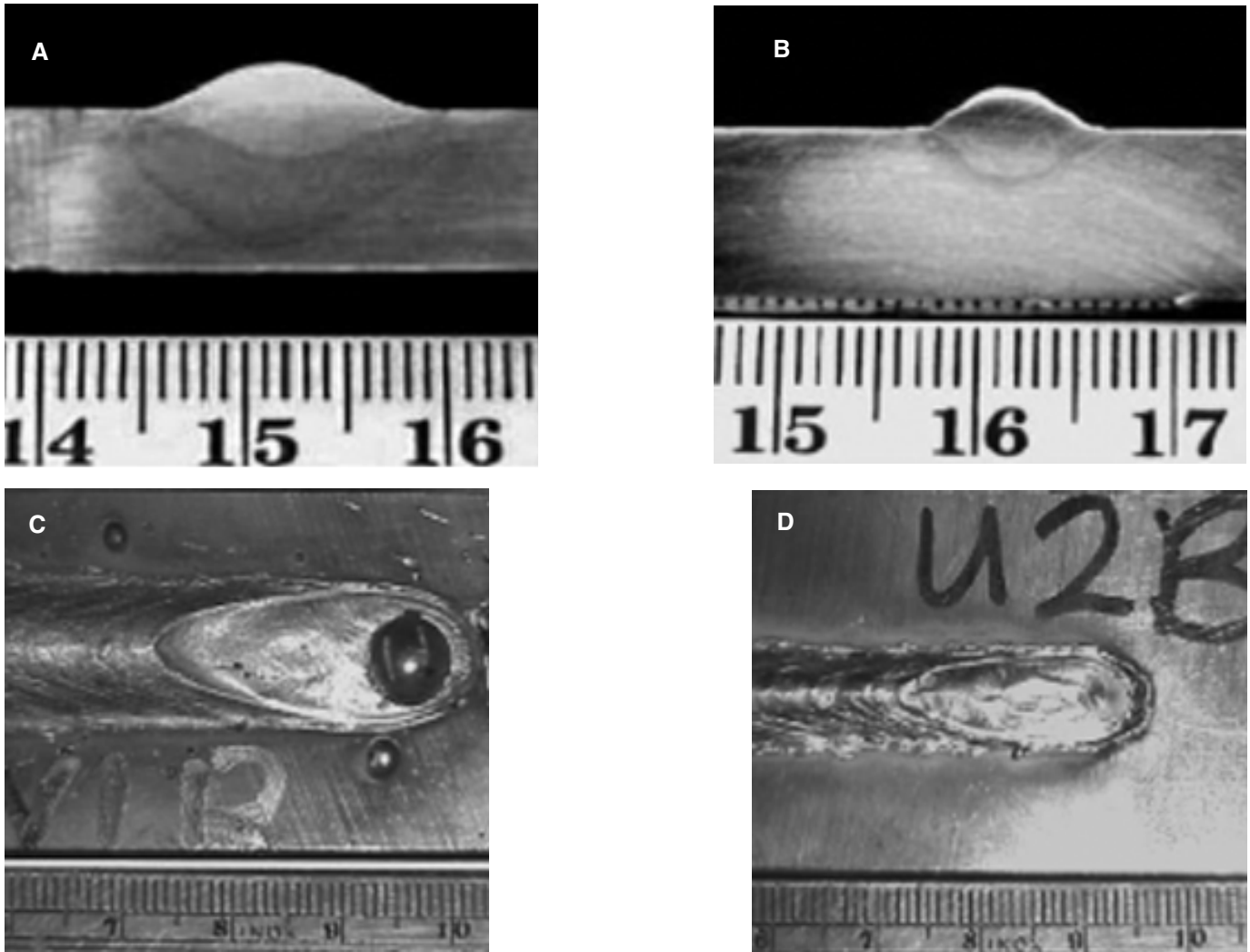


Fig. 10 — Macrographs of the welded specimens. A — Weld bead cross section V1B; B — weld bead cross section U2B; C — top view of the weld pool V1B; D — top view of the weld pool U2B

where  $r_f$  and  $r_b$  are proportion coefficients representing the heat apportionment in front and back of the double ellipsoidal heat source, respectively, and  $r_f + r_b = 2$ . Applying the continuity condition of the volume heat source for the plane  $x' = 0$ , the values of the heat density given by Equations 18A and B must be equal. Subsequently, the values of  $r_f$  and  $r_b$  can be evaluated as

$$r_f = \frac{2c_{hf} \cdot \left[ \operatorname{erf} \left( \frac{(L-x)\sqrt{3}}{c_{hf}} \right) + \operatorname{erf} \left( \frac{(L+x)\sqrt{3}}{c_{hf}} \right) \right]}{\left[ c_{hf} \cdot \left[ \operatorname{erf} \left( \frac{(L-x)\sqrt{3}}{c_{hf}} \right) + \operatorname{erf} \left( \frac{(L+x)\sqrt{3}}{c_{hf}} \right) \right] + c_{hb} \cdot \left[ \operatorname{erf} \left( \frac{(L-x)\sqrt{3}}{c_{hb}} \right) + \operatorname{erf} \left( \frac{(L+x)\sqrt{3}}{c_{hb}} \right) \right] \right]} \quad (19A)$$

$$r_b = \frac{2c_{hb} \cdot \left[ \operatorname{erf} \left( \frac{(L-x)\sqrt{3}}{c_{hb}} \right) + \operatorname{erf} \left( \frac{(L+x)\sqrt{3}}{c_{hb}} \right) \right]}{\left[ c_{hf} \cdot \left[ \operatorname{erf} \left( \frac{(L-x)\sqrt{3}}{c_{hf}} \right) + \operatorname{erf} \left( \frac{(L+x)\sqrt{3}}{c_{hf}} \right) \right] + c_{hb} \cdot \left[ \operatorname{erf} \left( \frac{(L-x)\sqrt{3}}{c_{hb}} \right) + \operatorname{erf} \left( \frac{(L+x)\sqrt{3}}{c_{hb}} \right) \right] \right]} \quad (19B)$$

It is worth noting here that this double ellipsoidal heat source for finite plate is described by five unknown parameters, which are the arc efficiency coefficient,  $\eta$ , and four other geometric parameters of the heat source:  $a_b$ ,  $b_h$ ,  $c_{hf}$ , and  $c_{hb}$ .

#### Analytical Approximate Solution for Double Ellipsoidal Heat Source in Finite Thick Plate

An analytical solution for the double ellipsoidal heat source is obtained by substituting heat density Equations 18A and B into Equation 5 and following a similar procedure as described in the section titled “Analytical Approximate Solution for Single Ellipsoidal Heat Source in Finite Thick Plate.” The transient temper-

ature for an arbitrary point  $(x,y,z)$  in a finite plate of length  $2L$ , width  $2B$ , and thickness  $D$ , subjected to the double ellipsoidal heat source is given as

$$T(x,y,z,t) - T_o = \frac{3\sqrt{3}Q}{2\rho c\pi\sqrt{\pi}} \int_0^t \left[ \frac{\exp\left(-\frac{3y^2}{12a(t-t') + a_h^2} - \frac{3z^2}{12a(t-t') + b_h^2}\right) \bullet E(B,y,a_h) \bullet E(D,z,b_h)}{\sqrt{12a(t-t') + a_h^2} \sqrt{12a(t-t') + b_h^2}} \right] \bullet dt' \quad (20)$$

$$\bullet \left[ \frac{r_f E(L, x-vt', c_{hf}) \exp\left(-\frac{3(x-vt')^2}{12a(t-t') + c_{hf}^2}\right)}{\sqrt{12a(t-t') + c_{hf}^2}} \right] \bullet dt'$$

$$+ \left[ \frac{r_b E(L, x-vt', c_{hb}) \exp\left(-\frac{3(x-vt')^2}{12a(t-t') + c_{hb}^2}\right)}{\sqrt{12a(t-t') + c_{hb}^2}} \right]$$

where  $E(L, x-vt', c_{hf})$ ,  $E(L, x-vt', c_{hb})$ ,  $E(B, y, a_h)$ , and  $E(D, z, b_h)$  are given by Equations 16B-D, respectively.

### Solution for Ellipsoidal Heat Sources in Dimensionless Form

The solution obtained for single and double ellipsoidal heat sources as shown in Equations 17 and 20 can be expressed further in much simpler dimensionless form by introducing the following dimensionless parameter variables as recommended by Christensen's method (Ref. 5):

- Dimensionless coordinates:  $\xi = vx/2a$ ,  $\psi = vy/2a$ ,  $\zeta = vz/2a$
- Dimensionless time:  $\tau = v^2(t-t')/2a$
- Dimensionless heat source parameters:  $u_a = va_h/(2a\sqrt{6})$ ,  $u_b = vb_h/(2a\sqrt{6})$ ,  $u_c = vc_{hf}/(2a\sqrt{6})$ , and  $u_{cb} = vc_{hb}/(2a\sqrt{6})$
- Dimensionless finite plate parameters: plate length,  $l = vL/2a$ ; plate width,  $b = vB/2a$ , and plate thickness,  $d = vD/2a$
- Dimensionless temperature:  $\theta = (T-T_o)/(T_c-T_o)$  where  $T_c$  is the reference temperature

- Christensen's operating parameter (Ref. 5):  $n = Qv/(4\pi a^2 \rho c (T_c - T_o))$

Substituting these parameters into Equations 17 and 20 and simplifying gives the following dimensionless form of the solutions for single and double ellipsoidal heat sources in finite plate, respectively, as

$$\frac{\theta}{n} = \frac{1}{\sqrt{2\pi}} \int_0^{\tau_{max}} \frac{e(l, \xi - \xi', u_c) \bullet e(b, \psi, u_a) \bullet e(d, \zeta, u_b)}{\sqrt{\tau + u_a^2} \sqrt{\tau + u_b^2} \sqrt{\tau + u_c^2}} \bullet \exp\left(\frac{(\xi - \xi')^2}{2(\tau + u_c^2)} - \frac{\psi^2}{2(\tau + u_a^2)} - \frac{\zeta^2}{2(\tau + u_b^2)}\right) d\tau \quad (21)$$

$$\frac{\theta}{n} = \frac{1}{2\sqrt{2\pi}} \int_0^{\tau_{max}} \frac{e(b, \psi, u_a) \bullet e(d, \zeta, u_b)}{\sqrt{\tau + u_a^2} \sqrt{\tau + u_b^2}} \bullet \exp\left(\frac{\psi^2}{2(\tau + u_a^2)} - \frac{\zeta^2}{2(\tau + u_b^2)}\right) d\tau$$

$$\bullet \left[ \frac{r_f e(l, \xi - \xi', u_{cf}) \exp\left(-\frac{(\xi - \xi')^2}{2(\tau + u_{cf}^2)}\right)}{\sqrt{\tau + u_{cf}^2}} \right]$$

$$\bullet \left[ \frac{r_b e(l, \xi - \xi', u_{cb}) \exp\left(-\frac{(\xi - \xi')^2}{2(\tau + u_{cb}^2)}\right)}{\sqrt{\tau + u_{cb}^2}} \right] \quad (22)$$

where  $l, b$ , and  $d$  are dimensionless length, width, and thickness of the plate [ $l = Lv/(2a\sqrt{6})$ ,  $b = Bv/(2a\sqrt{6})$  and  $d = Dv/(2a\sqrt{6})$ ];  $\tau_{max} = v^2t/2a$  and  $\xi = v^2t'/2a$  are the dimensionless time variables; and  $e(l, \xi - \xi', u_{cf})$ ,  $e(l, \xi - \xi', u_{cb})$ ,  $e(b, \psi, u_a)$ , and  $e(d, \zeta, u_b)$  are the correction terms for finite plate in dimensionless form as follows:

$$e(l, \xi - \xi', u_{cf}) = \text{erf}^{-1}\left(\frac{l}{u_{cf}\sqrt{2}}\right)$$

$$\bullet \left\{ \begin{aligned} &\text{erf}\left(\frac{l\sqrt{\tau + u_{cf}^2} + u_{cf}(\xi - \xi')}{u_{cf}\sqrt{2\tau} + \sqrt{2\tau}\sqrt{\tau + u_{cf}^2}}\right) \\ &+ \text{erf}\left(\frac{l\sqrt{\tau + u_{cf}^2} - u_{cf}(\xi - \xi')}{u_{cf}\sqrt{2\tau} - \sqrt{2\tau}\sqrt{\tau + u_{cf}^2}}\right) \end{aligned} \right\} \quad (23A)$$

$$e(l, \xi - \xi', u_{cb}) = \text{erf}^{-1}\left(\frac{l}{u_{cb}\sqrt{2}}\right)$$

$$\bullet \left\{ \begin{aligned} &\text{erf}\left(\frac{l\sqrt{\tau + u_{cb}^2} + u_{cb}(\xi - \xi')}{u_{cb}\sqrt{2\tau} + \sqrt{2\tau}\sqrt{\tau + u_{cb}^2}}\right) \\ &+ \text{erf}\left(\frac{l\sqrt{\tau + u_{cb}^2} - u_{cb}(\xi - \xi')}{u_{cb}\sqrt{2\tau} - \sqrt{2\tau}\sqrt{\tau + u_{cb}^2}}\right) \end{aligned} \right\} \quad (23B)$$

$$e(b, \psi, u_a) = \text{erf}^{-1}\left(\frac{b}{u_a\sqrt{2}}\right)$$

$$\bullet \left\{ \begin{aligned} &\text{erf}\left(\frac{b\sqrt{\tau + u_a^2} + u_a\psi}{u_a\sqrt{2\tau} + \sqrt{2\tau}\sqrt{\tau + u_a^2}}\right) \\ &+ \text{erf}\left(\frac{b\sqrt{\tau + u_a^2} - u_a\psi}{u_a\sqrt{2\tau} - \sqrt{2\tau}\sqrt{\tau + u_a^2}}\right) \end{aligned} \right\} \quad (23C)$$

$$e(d, \zeta, u_b) = \operatorname{erf}^{-1} \left( \frac{d}{u_b \sqrt{2}} \right) \cdot \left\{ \operatorname{erf} \left( \frac{d \sqrt{\tau + u_b^2}}{u_b \sqrt{2\tau}} - \frac{u_b \zeta}{\sqrt{2\tau} \sqrt{\tau + u_b^2}} \right) + \operatorname{erf} \left( \frac{u_b \zeta}{\sqrt{2\tau} \sqrt{\tau + u_b^2}} \right) \right\} \quad (23D)$$

and  $r_f$  and  $r_b$  become:

$$r_f = \frac{2 \cdot u_{hf} \cdot \operatorname{erf} \left( \frac{l}{u_{hf} \sqrt{2}} \right)}{u_{hf} \cdot \operatorname{erf} \left( \frac{l}{u_{hf} \sqrt{2}} \right) + u_{hb} \cdot \operatorname{erf} \left( \frac{l}{u_{hb} \sqrt{2}} \right)} \quad (24A)$$

$$r_b = \frac{2 \cdot u_{hb} \cdot \operatorname{erf} \left( \frac{l}{u_{hb} \sqrt{2}} \right)}{u_{hf} \cdot \operatorname{erf} \left( \frac{l}{u_{hf} \sqrt{2}} \right) + u_{hb} \cdot \operatorname{erf} \left( \frac{l}{u_{hb} \sqrt{2}} \right)} \quad (24B)$$

## Results and Discussion

### Numerical Procedure

In this study, a numerical procedure was applied to calculate the solution for the transient temperature field as described by Equations 16B–D and 20 for the double semi-ellipsoidal distributed heat source. A Fortran77 computer program was written to facilitate the integral calculation in Equation 20 and to allow for rapid calculation of geometry of the weld pool based on the assumed melting temperature of 1520°C for mild steel. Using this program, the effects of various heat source parameters ( $a_h$ ,  $b_h$ ,  $c_{hf}$ , and  $c_{hb}$ ) on the predicted weld pool geometry were investigated. The following material properties for high-strength steel were used for the calculation: heat capacity,  $c = 600 \text{ J/kg}^\circ\text{C}$ ; thermal conductivity,  $k = 29 \text{ J/m/s}^\circ\text{C}$ ; density,  $\rho = 7820 \text{ kg/m}^3$  (Ref. 4). Welding parameters used for calculation are voltage,  $U = 26 \text{ V}$ ; current,  $I = 230 \text{ A}$ ; welding speed,  $v = 30 \text{ cm/min}$ , and arc efficiency,  $\eta = 0.8$ .

### Transient Temperature Results

Using the above described numerical procedure, transient temperatures of three selected points  $A$ ,  $B$ , and  $C$  in a square steel plate  $240 \times 240 \times 20 \text{ mm}$  (as shown in Fig. 3) have been calculated and compared with the test results. The parameters of the double ellipsoids used for the calculation were estimated based on their relationship with the weld pool geometry measured after welding and calibrated with the measured temperature history. The best-fit values of the heat source parameters obtained for these test specimens are  $a_h = 7 \text{ mm}$ ,  $b_h = 2 \text{ mm}$ ,  $c_{hf} = 7 \text{ mm}$ ,  $c_{hb} = 14 \text{ mm}$ . More details about the test specimens and temperature measurement are described elsewhere (Ref. 2).

Figure 4 shows a comparison between the calculated transient temperatures at  $A$ ,  $B$ , and  $C$  and the measured ones based on the above-described heat source parameters, correspondingly. It can be seen from this figure that the calculated transient temperatures

are in good agreement with those measured in terms of both trends and magnitude. The predicted temperatures for weld toe point  $A$  shows steeper slope in cooling cycles compared with the corresponding measured temperatures. However, for point  $B$  the agreement between temperature slopes in the cooling cycles is quite reasonable. The predicted and measured temperatures at point  $C$  are in excellent agreement and the numerical results also show its kink point due to the corner position of point  $C$  as observed by the test.

If more sets of calibrated data are available, the relationship between the double ellipsoidal heat source parameters and the welding parameters such as  $U$ ,  $I$ ,  $v$  for a particular set of base and welding materials can be established and used for future heat source and welding simulation. This means that the approximate analytical solution for the developed heat source in finite thick plate can be used to simulate the transient temperatures of more complicated welding paths once the heat source parameters can be reliably predicted from the welding parameters for the associated welding materials and welding conditions.

### Simulated Weld Pool Results

In this work, a parametric study was carried out for various geometric parameters of the heat source to evaluate their influence on the simulated weld pool. Material properties and welding parameters were the same, as indicated in the section titled “Goldak’s Ellipsoidal Heat Sources in Semi-Infinite Body,” and kept unchanged for all simulations.

Figure 5A and B shows the effect of the heat source parameter  $a_h$  on the top view of the weld pool shape and its longitudinal cross section, respectively, while other heat source parameters are kept unchanged ( $b_h = 2 \text{ mm}$ ,  $c_{hf} = a_h \text{ mm}$ , and  $c_{hb}/c_{hf} = 2$ ). Figure 5A shows that as  $a_h$  increases from 1 to 5, the shape of the weld pool becomes shorter and fatter, i.e., its length decreases but its width increases. However, as  $a_h$  increases beyond a certain value ( $a_h > 5 \text{ mm}$ ), the weld pool becomes shorter and thinner.

This behavior of the heat source can be explained by the nature of the distributed heat source. This means that the higher the value of  $a_h$ , the weaker the heat density becomes. At the lower values of  $a_h$  ( $a_h < 5 \text{ mm}$ ), when the corresponding heat density is still high enough, the width of the weld pool increases as  $a_h$  increases and the weld pool length decreases for the same amount of heat input. At a higher value of  $a_h$  ( $a_h > 5 \text{ mm}$ ), the heat density decreases substantially and the same heat input will result in a lesser amount of melted metal, i.e., the smaller size of the weld pool. However, Fig. 5B shows the size of the weld pool in longitudinal cross section decreases as  $a_h$  increases, i.e., the pool depth decreases as  $a_h$  increases.

Figure 6A and B shows the effect of the heat source parameter  $b_h$  on the top view of the weld pool shape and its longitudinal cross section, while other heat source parameters are kept unchanged ( $a_h = 5 \text{ mm}$ ,  $c_{hf} = 5 \text{ mm}$  and  $c_{hb}/c_{hf} = 2$ ). It can be seen from that figure that as  $b_h$  increases from 1 to 8 mm, the pool length and width, as well as the weld pool depth, decreases. The effect of  $b_h$  of the heat source in finite plate on the weld pool geometry here is found much more pronounced than that of the heat source in semi-infinite body reported elsewhere (Ref. 2).

Figure 7A and B shows the effect of the heat source parameter  $c_{hf}$  on the top view of the weld pool shape and its longitudinal cross section, while other heat source parameters are kept unchanged ( $a_h = 5 \text{ mm}$ ,  $b_h = 2 \text{ mm}$ , and  $c_{hb}/c_{hf} = 2$ ). It can be seen from Fig. 7A that as  $c_{hf}$  increases from 1 to 10 mm, the weld pool width decreases, but its length increases while the weld pool depth decreases as in Fig. 7B. The increase in weld pool length is more pronounced at its front half than at its back half. The decrease in weld pool width is at a much lower magnitude. The behavior of the top view of the weld pool shape subjected to the  $c_{hf}$  is reflected on its longitudinal cross section as shown in Fig. 7B.

## Calibrated with the Measured Weld Pool

In this section, it will be shown that there is an alternative for establishing useful relationships between the double ellipsoidal heat source and the welding parameters, i.e., by calibrating the shapes of the measured and predicted weld pool using the heat source numerical solution. Similarly, once these relationships are established, the heat source parameters can be calculated from the welding parameters for a particular material and welding process and then be used for the welding simulation on the basis of the heat source solutions derived in this work.

**Welding Specimens.** Two different sets of gas metal arc (GMA) welding parameters were used to fabricate different shapes of weld bead that were run on top of the central line of two mild steel plates of  $375 \times 320 \times 10$  mm. A moving table with controlled travelling speed ( $v$ ) was set up under the welding gun of a GMAW machine. The welding system used for specimen fabrication and data acquisition is shown in Fig. 8A and B, respectively. The welding parameters, voltage ( $U$ ), current ( $I$ ), and welding wire feed rate ( $v_{feed}$ ), are controllable and monitored by means of a software called WeldPrint, which has been developed by the School of Electrical and Information Engineering, University of Sydney. The gas used for both sets of specimens was 100% CO<sub>2</sub> with a flow rate of 15 L/min. The welding parameters for two sets of specimens V1B and U2B are  $U = 31.9$  V,  $I = 110.7$  A,  $v = 5.9$  mm/s; and  $U = 24.9$  V,  $I = 169.9$  A, and  $v = 10.5$  mm/s, respectively, while the wire feed rate was kept the same at  $v_{feed} = 300$  in./min (127 mm/s).

**Calibrated Results.** Figure 9A and B shows comparisons between the measured and predicted data of top view of the weld pool shape on welded plate and its transversal cross section for both sets of welded specimens. The shapes of the weld pool and weld bead transversal cross section were measured directly from macrographs (as shown in Fig. 10) by means of a Windows®-based data collection program. The predicted data were calculated using the following heat source parameters for V1B and U2B specimens, which provide the best fit with the measured data.

- For the V1B specimen:  $a_h = 1$  mm,  $b_h = 6$  mm,  $c_{hf} = 7$  mm,  $c_{hb} = 15$  mm,  $\eta = 0.85$
- For the U2B specimen:  $a_h = 1$  mm,  $b_h = 3$  mm,  $c_{hf} = 5$  mm,  $c_{hb} = 10$  mm,  $\eta = 0.85$

These parameters were successfully selected based on the information of their effect on the weld pool geometry reported earlier. The heat transfer material properties used for the calculation were selected for mild steel (Ref. 6) as  $k = 40$  J/m/s°C,  $c = 639.4$  J/kg°C, and  $\rho = 7820$  kg/m<sup>3</sup>.

Figure 9A shows very good agreement between the measured and the predicted weld pool shape for both sets of welded specimens V1B and U2B, which represent two levels of heat input per unit of length  $q$  ( $q = UI\eta/v$ ) of 0.589 kJ/mm and 0.368 kJ/mm, respectively. It also shows that as the heat input,  $q$ , decreases the top view of the weld pool becomes shorter and narrower.

Figure 9B shows very reasonable agreement between the measured and the predicted shape of the weld bead cross section for both V1B and U2B. Figure 9B also shows that the depth of penetration increases as the welding current increases (from 110.7 to 169.9 A) despite the fact that the level of heat input  $q$  decreases (from 0.589 to 0.368 kJ/mm). This means that the effect of the welding current on weld bead penetration is stronger than that of the heat input per unit of length.

## Conclusions

Analytical approximate solutions for single and double ellipsoidal heat sources in finite thick plate have been derived and successfully calibrated with the test results. The solution for the double ellipsoidal heat source in finite thick plate was used to calculate transient temperatures at selected points in a steel plate

as well as carrying out the parametric study of the simulated weld pool. Very good agreement between the calculated and measured temperature data has been obtained and it has been shown that the predicted weld pool can be calibrated with the measured one by selecting suitable heat source parameters.

Once the relationships between the heat source and welding parameters can be established either by calibration with the measured temperature history or weld bead profile measurement, these can be effectively and conveniently used for various welding simulation purposes without the need to use the mirror method as required in the semi-infinite body. This solution could be used as a convenient tool for many problems in thermal stress analyses, residual stress analysis, and microstructure modeling of multipass welds.

## Acknowledgments

This work is currently sponsored by the University of Sydney's U2000 fellowship program. The authors would like to express their sincere thanks for the great support for this project provided by the School of Aerospace, Mechanical, and Mechatronic Engineering, University of Sydney. Special thanks are due to Prof. Ian H. Sloan, Department of Mathematics, University of New South Wales, for his useful comments during preparation of this paper and to Marcel H. Kaegi for his help in specimen fabrication.

## References

1. Goldak, J., Chakravarti, A., and Bibby, M. 1985. A double ellipsoid finite element model for welding heat sources. *IIW Doc. No. 212-603-85*.
2. Nguyen, N. T., Ohta, A., Matsuoka, K., Suzuki, N., and Maeda, Y. 1999. Analytical solution for transient temperature in semi-infinite body subjected to 3D moving heat sources. *Welding Journal* 78(8): 265-s to 274-s.
3. Nguyen, N. T., Ohta, A., Matsuoka, K., Suzuki, N., and Maeda, Y. 1999. Analytical solution of double-ellipsoidal moving heat source and its use for evaluation of residual stresses in bead-on-plate. *Proc. of Int. Conf. on Fracture Mechanics and Advanced Engineering Materials*. Editors: Lin Ye and Yiu Wing Mai, Dec. 8–10, 1999. University of Sydney, Australia, pp. 143–149.
4. Carslaw, H. S., and Jaeger, J. C. 1967. *Conduction of Heat in Solids*. Oxford University Press, pp. 255.
5. Christensen, N., Davies, V., and Gjermundsen, K. 1965. The distribution of temperature in arc welding. *British Welding Journal* 12(2):54-75
6. Radaj, D. 1992. *Heat Effects of Welding: Temperature Field, Residual Stress, Distortion*.

## Appendix A: Derivation of the Exact and Approximate Solution for Single Ellipsoidal Heat Source in Semi-infinite Body

### Exact Solution

Let us consider a single ellipsoidal heat source (Equation 10 in the main text) located in surface  $z = 0$  of semi-infinite body as in Fig. 1, the exact solution for the temperature field based on Equation 5 as described in the section titled "Temperature Field Solution Based on Green's Function for Instantaneous Point Source" as

$$\begin{aligned}
 & T(x, y, z, t) - T_o \\
 &= \frac{Q_{max}}{\rho c} \int_0^t dt' \int_{-\infty}^{\infty} dx' \int_{-\infty}^{\infty} dy' \int_0^{\infty} dz' \exp\left(-\frac{3x'^2}{c_h^2} - \frac{3y'^2}{a_h^2} - \frac{3z'^2}{b_h^2}\right) \\
 & \bullet G_{semi-inf}(x, y, z, t; x', y', z', t') dz' \quad (A1a)
 \end{aligned}$$

where  $Q_{max} = 6\sqrt{3} \cdot Q/a_h b_h c_h \pi \sqrt{\pi}$  for semi-infinite body and  $Q_{max} = 3\sqrt{3} \cdot Q/a_h b_h c_h \pi \sqrt{\pi}$  for infinite body;

$$G_{\text{semi-inf}}(x, y, z, t; x', y', z', t') = \frac{1}{[4\pi a(t-t')]^{3/2}} \bullet \exp\left[-\frac{(x-x')^2 + (y-y')^2}{4a(t-t')}\right] \bullet \left\{ \exp\left[-\frac{(z-z')^2}{4a(t-t')}\right] + \exp\left[-\frac{(z+z')^2}{4a(t-t')}\right] \right\} \quad (\text{A1b})$$

Substituting A1b for A1a and rearranging gives

$$T(x, y, z, t) - T_o = \int_0^t \frac{Q_{\text{max}}}{\rho c [4\pi a(t-t')]^{3/2}} dt' \int_{-\infty}^{\infty} \exp\left[-\frac{3x'^2}{c_h^2} - \frac{(x-x')^2}{4a(t-t')}\right] dx' \bullet \int_{-\infty}^{\infty} \exp\left[-\frac{3y'^2}{a_h^2} - \frac{(y-y')^2}{4a(t-t')}\right] dy' \bullet \int_{-\infty}^{\infty} \left\{ \exp\left[-\frac{3z'^2}{b_h^2} - \frac{(z-z')^2}{4a(t-t')}\right] + \exp\left[-\frac{3z'^2}{b_h^2} - \frac{(z+z')^2}{4a(t-t')}\right] \right\} dz' \quad (\text{A2})$$

Noting that

$$\int_{-\infty}^{\infty} \left\{ \exp\left[-\frac{3x'^2}{c_h^2} - \frac{(x-x')^2}{4a(t-t')}\right] \right\} dx' = \frac{c_h \bullet \sqrt{4a(t-t')}}{\sqrt{12a(t-t') + c_h^2}} \bullet \exp\left(-\frac{3x^2}{12a(t-t') + c_h^2}\right) \int_{-\infty}^{\infty} \exp(-u^2) du \quad (\text{A3a})$$

$$\int_{-\infty}^{\infty} \left\{ \exp\left[-\frac{3y'^2}{a_h^2} - \frac{(y-y')^2}{4a(t-t')}\right] \right\} dy' = \frac{a_h \bullet \sqrt{4a(t-t')}}{\sqrt{12a(t-t') + a_h^2}} \bullet \exp\left(-\frac{3y^2}{12a(t-t') + a_h^2}\right) \int_{-\infty}^{\infty} \exp(-v^2) dv \quad (\text{A3b})$$

$$\int_{-\infty}^{\infty} \left\{ \exp\left[-\frac{3z'^2}{b_h^2} - \frac{(z-z')^2}{4a(t-t')}\right] \right\} dz' = \frac{b_h \bullet \sqrt{4a(t-t')}}{\sqrt{12a(t-t') + b_h^2}} \bullet \exp\left(-\frac{3z^2}{12a(t-t') + b_h^2}\right) \int_{-w_0}^{\infty} \exp(-w^2) dw \quad (\text{A3c})$$

$$\int_{-\infty}^{\infty} \left\{ \exp\left[-\frac{3z'^2}{b_h^2} - \frac{(z+z')^2}{4a(t-t')}\right] \right\} dz' = \frac{b_h \bullet \sqrt{4a(t-t')}}{\sqrt{12a(t-t') + b_h^2}} \bullet \exp\left(-\frac{3z^2}{12a(t-t') + b_h^2}\right) \int_{w_0}^{\infty} \exp(-w^2) dw' \quad (\text{A3d})$$

where

$$u = \frac{x' \sqrt{12a(t-t') + c_h^2}}{c_h \sqrt{4a(t-t')}} - \frac{xc_h}{\sqrt{4a(t-t')} \sqrt{12a(t-t') + c_h^2}}$$

$$v = \frac{y' \sqrt{12a(t-t') + a_h^2}}{a_h \sqrt{4a(t-t')}} - \frac{ya_h}{\sqrt{4a(t-t')} \sqrt{12a(t-t') + a_h^2}}$$

$$w = \frac{z' \sqrt{12a(t-t') + b_h^2}}{b_h \sqrt{4a(t-t')}} - \frac{zb_h}{\sqrt{4a(t-t')} \sqrt{12a(t-t') + b_h^2}}$$

$$w' = \frac{z' \sqrt{12a(t-t') + b_h^2}}{b_h \sqrt{4a(t-t')}} + \frac{zb_h}{\sqrt{4a(t-t')} \sqrt{12a(t-t') + b_h^2}}$$

$$w_o = \frac{zb_h}{\sqrt{4a(t-t')} \sqrt{12a(t-t') + b_h^2}}$$

Making use of error function as

$$\text{erf}(b) = \frac{2}{\sqrt{\pi}} \int_0^b \exp(-t^2) dt$$

then Equations A3a and A3d can be simplified further as

$$\int_{-\infty}^{\infty} \left\{ \exp\left[-\frac{3x'^2}{c_h^2} - \frac{(x-x')^2}{4a(t-t')}\right] \right\} dx' = \frac{c_h \bullet \sqrt{4\pi a(t-t')}}{\sqrt{12a(t-t') + c_h^2}} \exp\left(-\frac{3x^2}{12a(t-t') + c_h^2}\right) \quad (\text{A4a})$$

$$\int_{-\infty}^{\infty} \left\{ \exp\left[-\frac{3y'^2}{a_h^2} - \frac{(y-y')^2}{4a(t-t')}\right] \right\} dy' = \frac{a_h \bullet \sqrt{4\pi a(t-t')}}{\sqrt{12a(t-t') + a_h^2}} \exp\left(-\frac{3y^2}{12a(t-t') + a_h^2}\right) \quad (\text{A4b})$$

$$\int_0^{\infty} \left\{ \exp\left[-\frac{3z'^2}{b_h^2} - \frac{(z-z')^2}{4a(t-t')}\right] \right\} dz' = \frac{b_h \bullet \sqrt{4\pi a(t-t')}}{2\sqrt{12a(t-t') + b_h^2}} \exp\left(-\frac{3z^2}{12a(t-t') + b_h^2}\right) \bullet [1 + \text{erf}(w_o)] \quad (\text{A4c})$$

$$\int_0^{\infty} \left\{ \exp \left[ -\frac{3z'^2}{b_h^2} - \frac{(z+z')^2}{4a(t-t')} \right] \right\} dz'$$

$$= \frac{b_h \cdot \sqrt{4\pi a(t-t')}}{2\sqrt{12a(t-t') + b_h^2}} \exp \left( -\frac{3z^2}{12a(t-t') + b_h^2} \right)$$

$$\bullet [1 - \text{erf}(w_0)] \quad (\text{A4d})$$

Substituting Equations A4a to A4d into Equation A2 and simplifying gives

$$T(x, y, z, t) - T_o = \frac{Q_{max} a_h b_h c_h}{\rho c}$$

$$\bullet \int_0^t \frac{\exp \left[ -\frac{3x^2}{12a(t-t') + c_h^2} - \frac{3y^2}{12a(t-t') + a_h^2} - \frac{3z^2}{12a(t-t') + b_h^2} \right] dt'}{\sqrt{12a(t-t') + a_h^2} \sqrt{12a(t-t') + b_h^2} \sqrt{12a(t-t') + c_h^2}} \quad (\text{A5})$$

Substituting the value  $Q_{max} = 6\sqrt{3} \cdot Q / (a_h b_h c_h \pi \sqrt{\pi})$  for semi-infinite body into Equation A5 and further simplifying gives

$$T(x, y, z, t) - T_o = \frac{3\sqrt{3}Q}{\rho c \pi \sqrt{\pi}}$$

$$\bullet \int_0^t \frac{\exp \left[ -\frac{3x^2}{12a(t-t') + c_h^2} - \frac{3y^2}{12a(t-t') + a_h^2} - \frac{3z^2}{12a(t-t') + b_h^2} \right] dt'}{\sqrt{12a(t-t') + a_h^2} \sqrt{12a(t-t') + b_h^2} \sqrt{12a(t-t') + c_h^2}} \quad (\text{A6})$$

This is the exact solution for a single ellipsoidal heat source in the semi-infinite body derived by using the respective Green's function for a point heat source.

### Approximate Solution Using the Effective Heat Source and Green's Function for a Point Heat Source in an Infinite Body

Now let us consider the same single ellipsoidal heat source in a semi-infinite body but try to solve it by using the approximate approach as described in the section titled "Approximate Approach for Temperature Field Subjected to Volume Heat Source in Finite Body" in the main text of this paper, according to which the approximate solution for this heat source is given by Equation 6 as

$$T(x, y, z, t) - T_o = \frac{Q_{max, semi-inf}}{\rho c}$$

$$\bullet \int_0^t dt' \int_{-\infty}^{\infty} dx' \int_{-\infty}^{\infty} dy' \int_0^{\infty} \exp \left( -\frac{3x'^2}{c_h^2} - \frac{3y'^2}{a_h^2} - \frac{3z'^2}{b_h^2} \right)$$

$$\bullet G_{inf}(x, y, z, t; x', y', z', t') dz' \quad (\text{A7a})$$

$$\text{where } Q_{max, semi-inf} = \frac{6\sqrt{3} \cdot Q}{a_h b_h c_h \pi \sqrt{\pi}} \quad (\text{A7b})$$

for semi - infinite.

$$G_{inf}(x, y, z, t; x', y', z', t') = \frac{1}{[4\pi a(t-t')]^{3/2}}$$

$$\bullet \exp \left[ -\frac{(x-x')^2 + (y-y')^2 + (z-z')^2}{4a(t-t')} \right] \quad (\text{A7c})$$

Similarly, substituting A7b and A7c to A7a and rearranging gives

$$T(x, y, z, t) - T_o = \int_0^t \frac{Q_{max, semi-inf}}{\rho c [4\pi a(t-t')]^{3/2}} dt'$$

$$\bullet \int_{-\infty}^{\infty} \exp \left[ -\frac{3x'^2}{c_h^2} - \frac{(x-x')^2}{4a(t-t')} \right] dx' \int_{-\infty}^{\infty} \exp \left[ -\frac{3y'^2}{a_h^2} - \frac{(y-y')^2}{4a(t-t')} \right] dy'$$

$$\bullet \int_0^{\infty} \exp \left[ -\frac{3z'^2}{b_h^2} - \frac{(z-z')^2}{4a(t-t')} \right] dz'$$

Substituting Equations A4a to A4c and A7b into Equation A8 and simplifying gives

$$T(x, y, z, t) - T_o = \frac{3\sqrt{3}Q [1 + \text{erf}(w_0)]}{\rho c \pi \sqrt{\pi}}$$

$$\bullet \int_0^t \frac{\exp \left[ -\frac{3x^2}{12a(t-t') + c_h^2} - \frac{3y^2}{12a(t-t') + a_h^2} - \frac{3z^2}{12a(t-t') + b_h^2} \right] dt'}{\sqrt{12a(t-t') + a_h^2} \sqrt{12a(t-t') + b_h^2} \sqrt{12a(t-t') + c_h^2}} \quad (\text{A9})$$

Equation A9 gives the approximate solution for the single ellipsoidal heat source in a semi-infinite body. It is worth noting here that the temperature field given by the approximate solution is increased by a factor of  $(1 + \text{erf}(w_0))$  compared to that given by the exact solution as in Equation A6 where

$$w_o = \frac{zb_h}{\sqrt{4a(t-t')} \sqrt{12a(t-t') + b_h^2}}$$

The value of error function  $\text{erf}(w_0)$  becomes zero ( $\text{erf}(w_0)=0$ ) when  $z=0$ , i.e., the approximate solution becomes the exact one at the surface of a semi-infinite body. In general, the value of error function varies between 0 and 1 ( $0 \leq \text{erf}(w_0) \leq 1$ ) and for a certain time ( $t-t'$ ) it increases as  $z$  increases, i.e., the approximate solution would overpredict the temperature field in the thickness direction.

It is worth noting here that the shape of the temperature field in a semi-infinite body obtained by the approximate approach is the same as that by the exact solution.